
Silicon Detector (SiD) Tracking Geometry Optimization Studies for the ILC

S. U. Setru¹ and M. Demarteau^{*1}

¹Argonne National Laboratory, 9700 South Cass Avenue, IL, USA

Abstract

We studied modifications to the tracking system of the baseline Silicon Detector (SiD) geometry for the proposed International Linear Collider (ILC) as presented in the SiD Detailed Baseline Design (DBD) [1]. The vertex barrel has five roughly evenly spaced tracking layers. The spatial arrangement of the vertex barrels was modified to three sets of two closely-spaced tracking layers. The tracking performance was studied using Monte Carlo simulations of single muons and two physics processes, $e^+e^- \rightarrow t\bar{t}$ at $\sqrt{s} = 500$ GeV and $e^+e^- \rightarrow t\bar{t}b\bar{b}$ (hadronic decays only) at $\sqrt{s} = 1$ TeV. The modified detector has greater z -axis impact parameter resolution for high polar angles ($\theta > 60^\circ$) for single muons at 10 and 100 GeV. The modified detector has lower efficiency for low energy single muons in the forward region. In the central region, the modified detector has better z -axis impact parameter resolution but worse transverse impact parameter resolution for high energy muons. For the two physics processes, the modified detector has higher efficiency for low energy particles, lower efficiency for high energy particles, and lower efficiency as a function of the number hits produced by the reconstructed Monte Carlo charged particles. The modified detector also has higher track fake rates for both physics processes for a wide range of polar angle and transverse momentum. In all other aspects of detector performance, both detectors performed comparably. Neither detector geometry performed unequivocally better than the other for the parameter space studied.

1 Introduction

The International Linear Collider (ILC) is a proposed e^+e^- collider with a center of mass energy of up to 1 TeV that will enable the particle physics community

^{*}Corresponding author: demarteau@anl.gov



to perform precision studies of the Higgs boson and search for physics beyond the Standard Model [2]. The physics goals of the ILC necessitate the development of collider detectors with unprecedented charged particle tracking capabilities [1]. Two different detector designs have been put forward for the ILC, the International Large Detector (ILD) and the Silicon Detector (SiD). ILD uses a time projection chamber to provide continuous charged particle tracking and a very low material budget between the interaction point and the calorimeter [1]. SiD uses all-silicon tracking in a 5 Tesla magnetic field, resulting in a compact and cost-controlled detector that has excellent tracking performance and can mitigate e^+e^- pair background [1]. The ILC has been designed such that both detectors alternately share the same interaction point via the so-called “push-pull” system, in which one detector slides out to accommodate the other [1]

It is crucial that the design of the tracking system be optimized with respect to various parameters, including but not limited to material budgets, segmentation [3], and tracker geometry. This paper presents tracking performance studies optimizing the vertex detector geometry of the SiD baseline design, ‘Sidlo3’ (figure 1), as presented in the SiD detailed baseline document (DBD) [1]. We first provide an overview of Sidlo3’s tracking systems, and then present the vertex barrel geometry modification which was investigated. We only modified the geometry of the barrels of the vertex detector. We then discuss our simulation, reconstruction, and analysis methods and present the tracking performance of the modified vertex barrel in comparison to the tracking performance of the Sidlo3 detector.

2 Baseline Tracking System

The silicon single length crossing time stamping as implemented by Sidlo3 include robust handling of the ILC beam background and outstanding momentum resolution for charged particles [1]. Sidlo3 uses all-silicon tracking with pixel segmentation in the vertex barrels and disks, and strip segmentation in the tracker barrels and disks [1]. The entire tracker is shown in figure 1 and each subdetector’s coverage as a function of polar angle is shown in figure 4a. Details concerning the segmentation and readout dimensions used for this study may be found in section 3.2. For a more detailed look at each of the tracking systems as well as hardware and electronics research and development, see [1].

2.1 Sidlo3 Baseline Vertex Detector

The vertex detector of Sidlo3 (figure 2) has been designed so as to have excellent tracking precision and a very low material budget, to reduce the effects from multiple

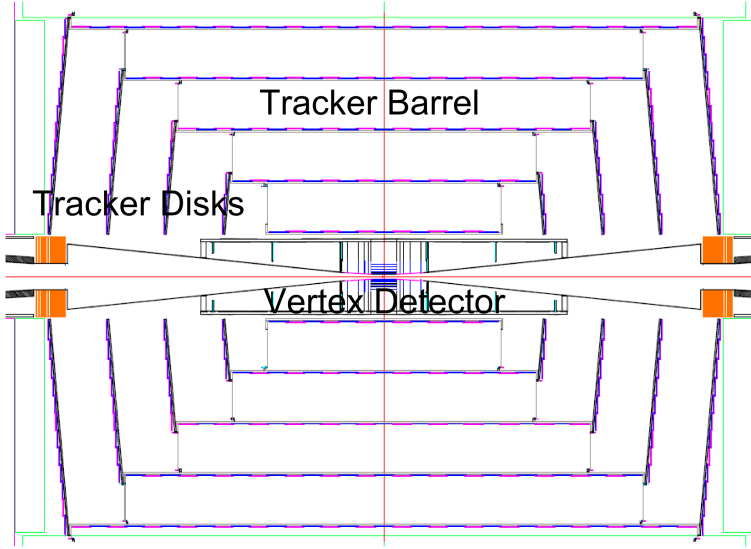


Figure 1: The entire Sidlo3 tracker. A more detailed sketch of the vertex subdetectors is given in figure 2. The figure is taken from the SiD DBD [1].

Coulomb scattering. Sidlo3’s vertex detector includes barrel layers wrapping around the interaction point, inner disks close to the interaction point (small z), and outer disks away from the interaction point (large z). All tracking parts of the vertex detector feature $20 \times 20 \mu\text{m}^2$ pixel segmentation. The vertex detector is arranged so as to provide broad coverage for a wide polar angle, $\cos \theta \approx 0.984$ [1]. The polar angle coverage of Sidlo3’s vertex tracking systems is illustrated in figure 4a. Note that figure 4a also includes the coverage of the outer trackers (figure 1, which are further from the interaction point than the vertex detectors).

2.2 Vertex Barrel Geometry Modification

The Sidlo3 vertex barrel geometry consists of five pixellated layers, as illustrated in figure 3a. The modified geometry that we studied consists of six such layers grouped into three sets of two “doublet” layers, as illustrated in figure 3b, with a gap of 3 mm between layers in each doublet. Table 1 gives some of the geometry parameters of the two different radial barrels. The modified geometry keeps layers one, three, and five in the same position as in Sidlo3. The modified geometry also keeps the same thickness and segmentation of the modules comprising the vertex barrel. The width of the tracker module remains the same for most layers except layers two and four. For two and four, the module is wider by 1 mm in order to insure proper overlap at the module junctions at a greater radial distance from the interaction point. The ϕ rotation for detector modules and the number of modules are kept the same for

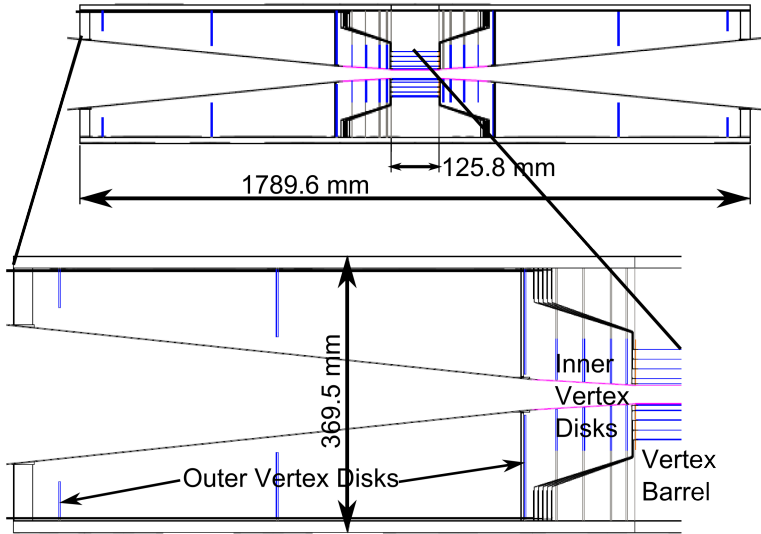


Figure 2: The vertex barrel, inner, and outer disks in the Sidlooi3 detector [1].

layers within each doublet. No other modifications were made to the vertex barrel of Sidlooi3 or to any other part of the Sidlooi3 detector. Figure 4 illustrates the coverage of the tracking systems as a function of polar angle for both detectors. Notice that the coverage for all tracking systems increased the number of hits in the vertex detector at large angle.

3 Methods and Software

Monte Carlo physics events and single muons were simulated using the Simulator for the Linear Collider (SLIC) [4] program, which uses the GEANT4 toolkit [5,6] as the underlying physics engine. The org.lcsim software framework [7,8] reconstructs the simulated events by first digitizing the simulated tracker hits and then building tracks from these hits, as described in section 3.2. Finally, the Monte Carlo true information and the reconstructed data are analyzed and compared to determine each detector’s performance. Simulation, reconstruction, and analysis were performed on the grid using ILCDIRAC version 6.8.28 [9], which is an extension of the DIRAC framework [10]. The full software pipeline is illustrated in figure 5. The next section describes the different steps in more detail.

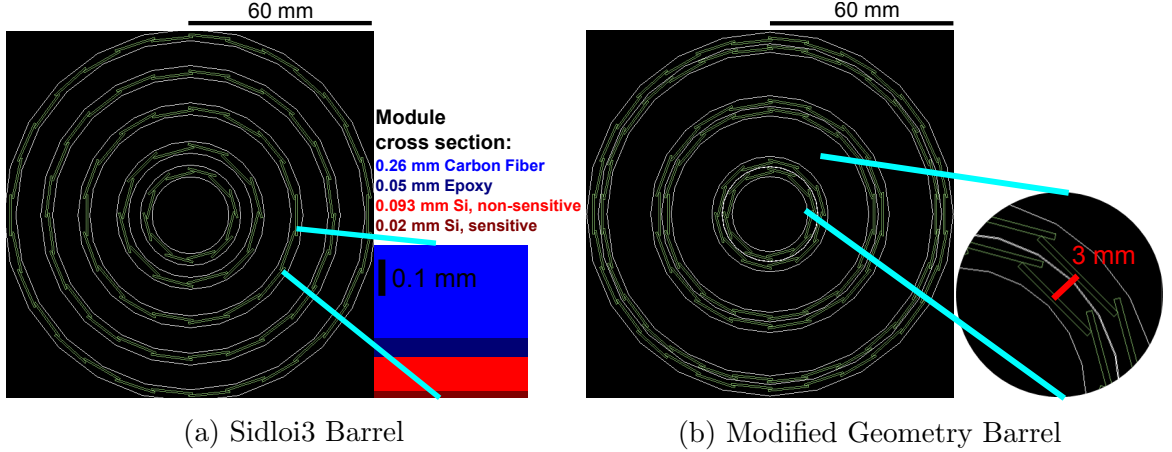


Figure 3: View of the $r\phi$ plane (a) Sidlo3’s vertex barrel and (b) the modified barrel. The green boxes depict individual detector modules. The white lines surrounding each layer depict the detector envelopes as defined in SLIC. The detail in (a) shows, to scale, the various material thicknesses of the module used in the vertex barrels. Every module in both vertex barrels share the same material budget. Note that the detail in (a) is only to scale in the vertical dimension, not longitudinally.

Detector	Layer	Radius (mm)	Module Dimensions (mm)
Sidlo3	1	15.05	$9.6 \times 125.0 \times 0.873$
	2	23.03	$13.8 \times 125.0 \times 0.873$
	3	35.79	$13.8 \times 125.0 \times 0.873$
	4	47.50	$13.8 \times 125.0 \times 0.873$
	5	59.90	$13.8 \times 125.0 \times 0.873$
Modified Detector	1	15.05	$9.6 \times 125.0 \times 0.873$
	2	18.05	$10.6 \times 125.0 \times 0.873$
	3	35.79	$13.8 \times 125.0 \times 0.873$
	4	38.79	$14.8 \times 125.0 \times 0.873$
	5	56.90	$13.8 \times 125.0 \times 0.873$
	6	59.90	$13.8 \times 125.0 \times 0.873$

Table 1: Comparison of the geometry specifications for the vertex barrel of Sidlo3 (figure 3a) and the modified detector (figure 3b). The modified detector has a 3 mm gap in radius between layers 1 and 2, 3 and 4, and 5 and 6. In the modified detector, the module width increases by 1 mm in layers 2 and 4. Also notice that the thickness (0.873 mm) and depth in z (125.0 mm) remains the same in both detectors.

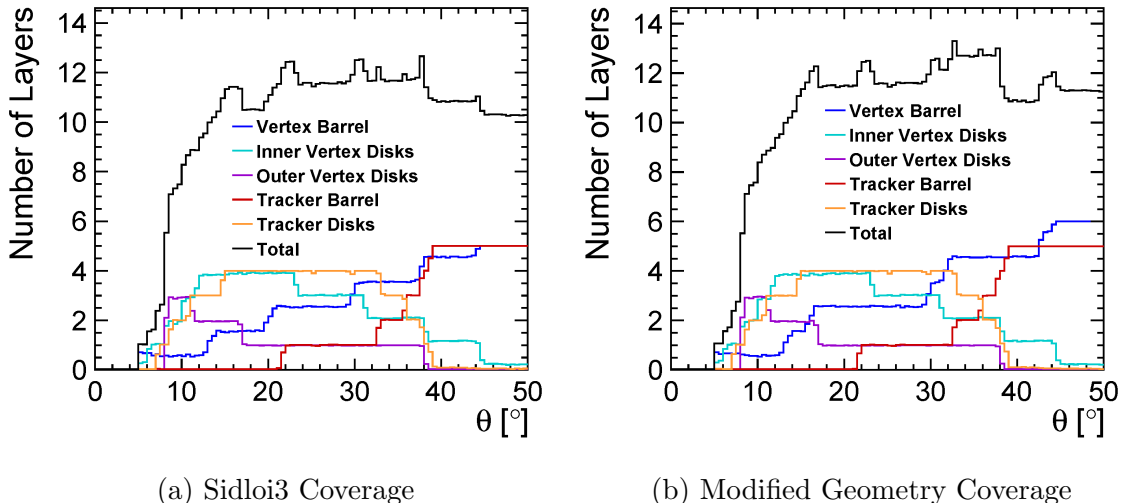


Figure 4: Coverage of the tracking systems as a function of polar angle for (a) Sidlo3 and (b) the modified detector. Comparison of the figures illustrates the difference in the coverage of the vertex barrel. Most noticeably, for high polar angles, the vertex barrel reaches a peak of six layers in the modified geometry as expected, whereas Sidlo3 reaches a peak of five layers. Coverage is the same for all other tracking systems.

3.1 Detector, Single Particle, and Physics Simulation

SLIC accepts detector geometry definitions in an extensible markup language (XML) format. The XML description for the modified geometry was made using Sidlo3’s XML description as a template, since both detectors are exactly the same except for the vertex barrel. SLIC produces simulation files in the Linear Collider Input/Output (LCIO) [11] file format. Simulations utilized SLIC version 3.0.3.

Tracking performance studies were conducted using simulations of single muons, $e^+e^- \rightarrow t\bar{t}$ events at $\sqrt{s} = 500$ GeV, and $e^+e^- \rightarrow t\bar{t}b\bar{b}$ (hadronic decays only) events at $\sqrt{s} = 1$ TeV. Initial particle four-vectors for the two physics processes were provided as a STDHEP file [12], while GEANT4’s General Particle Source (GPS) allows for simulation of muons at user-defined, fixed energies and angles or user-defined energy and angular distributions. The physics event samples were generated using the WHIZARD [13] event generator, with hadronization of quarks performed by PYTHIA [14], as described in [15,1]. Our studies did not include simulations of beam-induced backgrounds.

GEANT4 propagates the simulated particles through each layer of the detector discretely, calculating the interaction between each particle and the material of each layer in order to determine the energy loss and the particle’s new position and momen-

tum. Geant4 knows where to search for material according to the spatial boundaries established by the detector envelopes, which are shown by white lines in figure 3. The description of each particle’s interaction with the materials in the layers is determined by a user-defined reference physics list. The GEANT4 QGSP_BERT physics list [16] was used to determine particle interactions with matter, which has been shown to agree well with beam tests [17]. In those parts of a layer which have been designated as ‘sensitive’ (figure 3a), the energy left by a particle is recorded as a ‘hit’.

3.2 Tracker Hit Digitization and Event Reconstruction

The org.lcsim software framework [7,8] digitizes the hits and reconstructs events. Tracker hit digitization, performed by the *SiSim* package in org.lcsim, converts the energy deposits from the simulation step into digital signals, one per channel [15]. Charged particle tracks are then reconstructed from these hits using the *SeedTracker* algorithm in org.lcsim, which finds tracks according to user-generated, detector-specific tracking strategies [15]. (See section 3.2.1.) The output LCIO file from org.lcsim contains the reconstructed tracks and their parameters, the Monte Carlo true parameters for each simulated particle, and relational tables between each reconstructed tracker hit and the Monte Carlo particle associated with it, which allows the analysis of tracking performance. Our studies used org.lcsim 2.5.

The segmentation of the various tracking layers is implemented after the simulation and during the reconstruction step using Java drivers [15]. For pixel sensors, both the sensor and readout pitches are set to $20\ \mu m$ in x and y . Pixellated segmentation is used in the vertex barrels and disks. For strip sensors, which run parallel to the global z -axis, the sensor pitch is set to $25\ \mu m$ and the readout pitch is set to $50\ \mu m$. Thus, every other strip is directly read out. The intermediate strip is coupled capacitively to the readout strips [18]. The segmentation along the section is 10 cm,

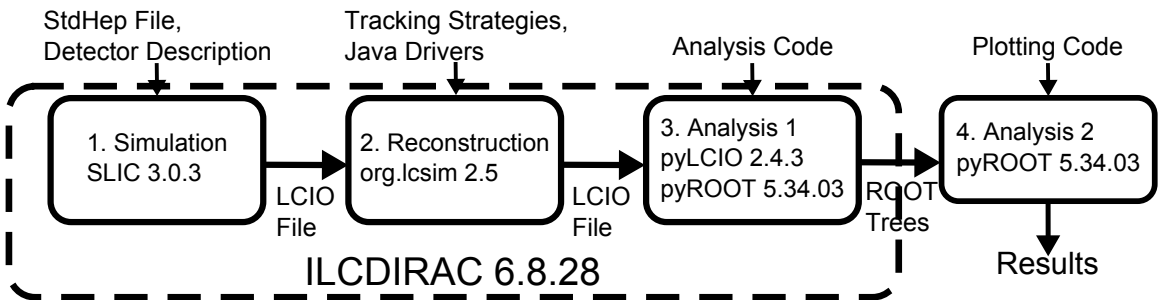


Figure 5: The software pipeline for the tracking studies. Note that steps one, two, and three are all performed on the grid via ILCDIRAC version 6.8.28. The last step is performed locally.

the length of the sensor. Strip segmentation is used in the tracker barrels and disks. A nearest neighbor algorithm clusters digitized hits that are near each other [15]. These clusters of hits form the tracking hits which the *SeedTracker* algorithm uses to reconstruct tracks. In the LCIO data model, five unique geometric parameters define a helix [19]. Using the L3 convention [20], these parameters are d_0 , κ , ϕ_0 , $\tan \lambda$, and z_0 , illustrated in figure 6. From these helix parameters, the track's physical quantities may be determined according to the following equations [15].

$$\begin{aligned} p_T &= kB/|\kappa|, \quad k = 0.003 \text{ GeV T}^{-1} \text{ mm}^{-1} \\ p_x &= p_T \cos \phi_0 \\ p_y &= p_T \sin \phi_0 \\ p_z &= p_T \tan \lambda \\ p &= p_T / \cos \lambda \\ q &= \kappa / |\kappa| \end{aligned}$$

For a discussion of the uncertainty in the track parameters and their propagation, see [15].

3.2.1 Tracking Strategies

The *SeedTracker* algorithm relies on a group of tracking strategies to reconstruct tracks. Each tracking strategy is a set of tracker layers from which the algorithm must use tracker hits to produce the reconstructed helical tracks of charged particles. Each reconstructed track produced by a given strategy must satisfy the track parameter and helix fit requirements listed in table 2. Each strategy assigns one of three roles to each tracking layer: seeding, confirming, and extending. In any given strategy, there are 3 seed layers, 1 confirm layer, and any additional number of extend layers. All combinations of hits from the 3 seed layers form the initial set of possible tracks. An initial helix fit to each candidate determines the track parameters. Then, each candidate is tested with each hit in the confirm layer for another helix fit and only those hits are kept whose addition to the fit keeps $\chi^2 < \chi^2_{max}$, one of the cuts listed in table 2. Only those hits in the confirm layer whose position in ϕ and z are consistent with a given candidate's initial parameters are tested. Multiple confirmed seeds from a single possible track are possible. Finally, each seed is extended layer by layer using the hits in the extend layers, so long as the various cuts specified in table 2 are still met. As with the confirm layer, only hits with ϕ and x positions plausible for the given track are tested. Once there are not enough layers remaining for a seed track to satisfy N_{min} , that track is discarded. If the track being reconstructed shares more than one hit in common with a previously reconstructed track, the track with more

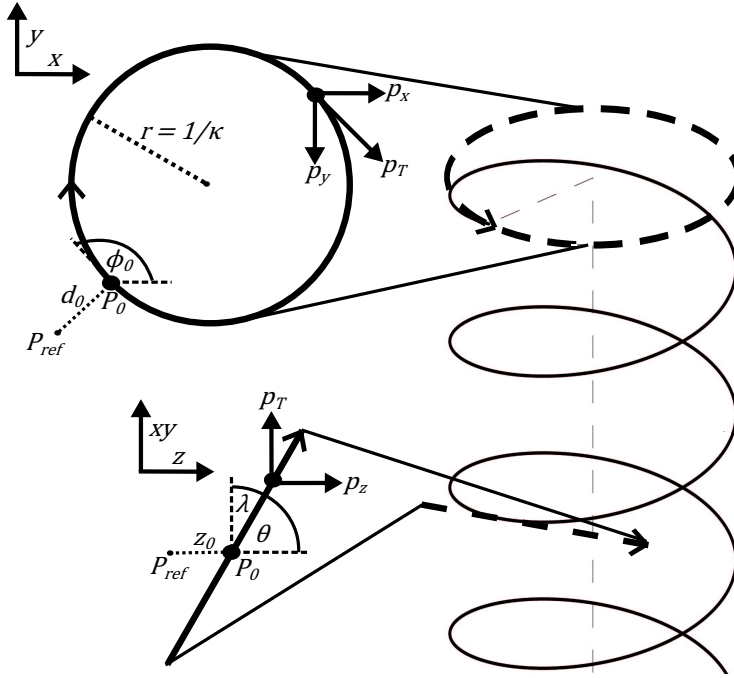


Figure 6: LCIO track parameter definition. Parameters are defined with respect to P_{ref} , which we place for convenience at the origin (0,0,0). Point P_0 , with coordinates (x_0, y_0, z_0) , marks the starting point of the helix, which is the track's xy projection's closest point of approach to P_{ref} . The xy impact parameter d_0 is given by $d_0 = \sqrt{x_0^2 + y_0^2}$. From the track parameters, physical parameters may be calculated via equations ??.

hits is kept or, in the case of tracks with equal hit numbers, the track with lowest χ^2 . For details concerning the helix fitting and accounting of multiple scattering, see [15].

Tracking strategies may be produced manually by creating lists of seed, confirm, and extend layers with which one would like reconstruct tracks. However, the preferable manner for making strategies involves generating the strategies via an org.lcsim software tool and a sample physics process with the required angular and energy distributions [15]. Ideally, the sample physics process used to build the strategies should densely populate the phase space. For our tracking studies, two sets of strategies were generated, one using $500 e^+e^- \rightarrow t\bar{t}$ events at $\sqrt{s} = 500$ GeV and another using $500 e^+e^- \rightarrow t\bar{t}b\bar{b}$ (hadronic decays only) events at $\sqrt{s} = 1$ TeV. The $t\bar{t}$ -generated strategies were used to reconstruct single muon tracks and $t\bar{t}$ events. The $t\bar{t}b\bar{b}$ -generated strategies were used to reconstruct $t\bar{t}b\bar{b}$ events.

Track, Fit Parameters	Barrel Only Strategy	All Other Strategies
N_{min}	6	7
$p_{T,min}$	0.2	0.2
$d_{0,max}$	5.0	10.0
$z_{0,max}$	10.0	10.0
χ^2_{max}	10.0	50.0

Table 2: Cuts on several reconstructed track parameters and the χ^2 of the helix fit. The cuts are passed to the tracking strategies to define acceptable reconstructed tracks. N_{min} refers to the minimum number of hits required for a reconstructed track. Refer to figure 6 to see the track parameters p_T , d_0 , and z_0 illustrated. The barrel only strategy is designed for finding low p_T tracks at high polar angles whose radius of curvature is lower than the seventh tracker layer. It requires only six hits but uses a more strict χ^2 cut than that used for all other strategies. The effect of varying the N_{min} and χ^2 cut on tracking efficiency is shown in [15]

3.3 Analysis

The output LCIO files from org.lcsim were analyzed using Python code. ROOT trees were generated by linking the pyLCIO and pyROOT bindings to the respective LCIO and ROOT C++ libraries. Each ROOT tree contains the helix and physical parameters for both the Monte Carlo particles and the reconstructed tracks. The trees also map tracks to the Monte Carlo particles, allowing for the comparison between the Monte Carlo truth of helix and physical parameters with their reconstructed values. Such comparisons enable study of the tracking performance of each detector. The ROOT trees, which are produced on the grid via ILCDIRAC, are then downloaded locally and further analyzed to produce the final results.

4 Tracking Performance Results

4.1 Tracking Efficiency

Tracking efficiency is defined as the fraction of findable charged particles that were successfully reconstructed:

$$\text{Efficiency} = \frac{N_{\text{successfully reconstructed}}}{N_{\text{findable}}}. \quad (1)$$

Findable particles are charged particles originating within $\pm 5\text{ cm}$ from the interaction point that travel a line-of-sight distance $> 5\text{ cm}$. A track is truth matched to the

Monte Carlo particle that contributed the majority of hits. In addition, only tracks with at most one falsely assigned hit are considered successfully reconstructed.

4.1.1 Single Muons

As shown in figure 7, the baseline and modified detectors had nearly 100% efficiency for $\theta > 30^\circ$ for 1 GeV (figure 7a), 10 GeV (figure 7b), and 100 GeV (figure 7c) muons. For 10 GeV and 100 GeV muons, both detectors also had nearly identical efficiencies for $\theta < 30^\circ$. However, for 1 GeV at $\theta < 30^\circ$, the modified detector performed slightly worse (figure 7a). Sidlo3 maintained an efficiency near 100%, whereas the modified detector's efficiency dipped to as low as 95%.

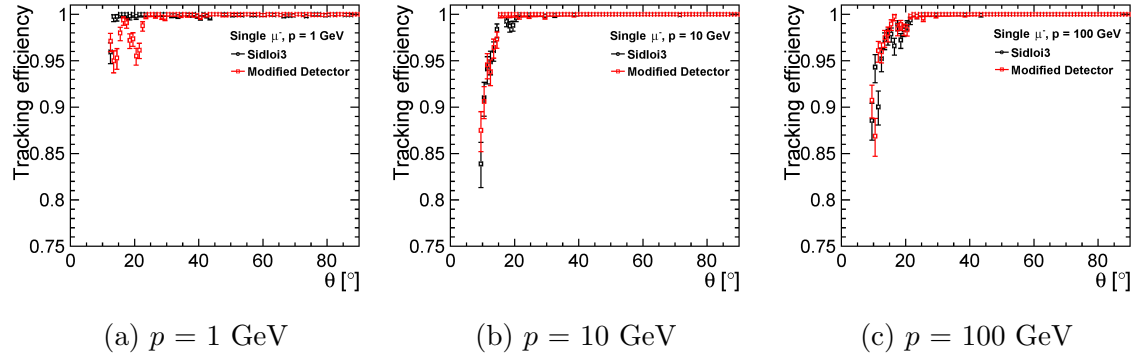


Figure 7: Tracking efficiency for single muons as a function of polar angle for (a) 1 GeV, (b) 10 GeV, and (c) 100 GeV muons.

In figure 8, the tracking efficiency has been plotted with respect to the transverse momentum for various polar angles. The difference in performance between the two detectors is less clear. Still, there is a slight dip in the modified detector's efficiency for low transverse momentum muons ($p_T < 0.5 \text{ GeV}$) at $\theta = 15^\circ$ (figure 8a) and $\theta = 30^\circ$ (figure 8b), echoing the results from figure 7a. Also, for $\theta = 90^\circ$ (figure 8c), both detectors have identical performance for the full range of transverse momentum.

4.1.2 $e^+e^- \rightarrow t\bar{t}$, $\sqrt{s} = 500 \text{ GeV}$

For $e^+e^- \rightarrow t\bar{t}$ events, the modified detector demonstrated greater efficiency than Sidlo3 for lower transverse momentum particles ($0.5 \text{ GeV} < p_T < 30 \text{ GeV}$) for $\theta > 30^\circ$, as illustrated in figure 9a and figure 9b. On the other hand, as shown in figure 9c,

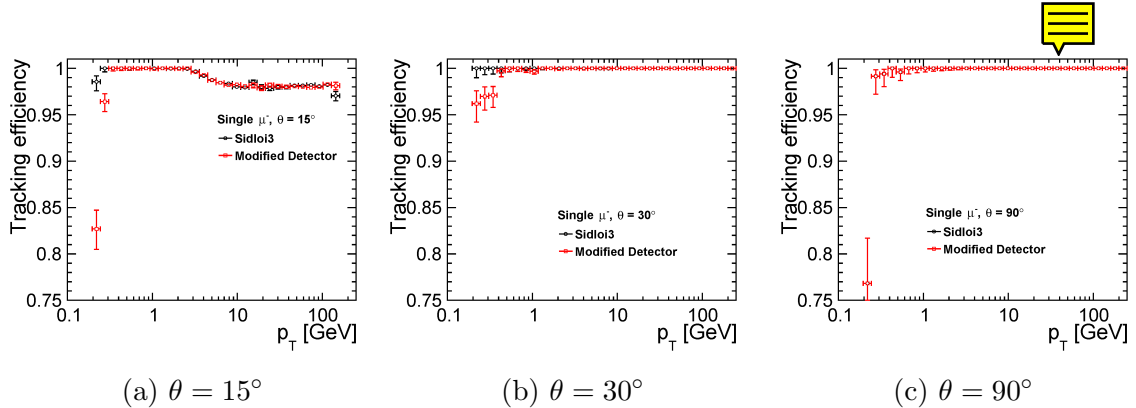


Figure 8: Tracking efficiency for single muons as a function of transverse momentum for muons at (a) $\theta = 15^\circ$, (b) $\theta = 30^\circ$, and (c) $\theta = 90^\circ$.

the modified detector had slightly worse efficiency than Sidlo3 for higher transverse momentum particles ($30 \text{ GeV} < p_T$) at $\theta > 60^\circ$. The distinction between both detectors blurs for low polar angles ($\theta < 30^\circ$).

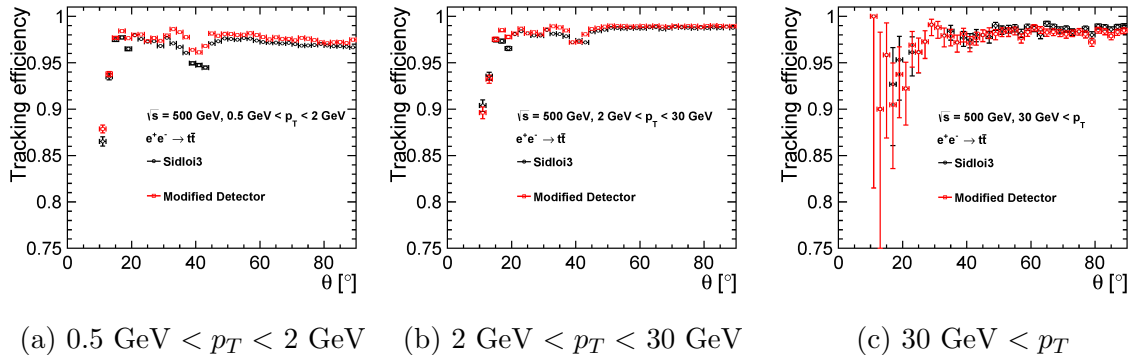


Figure 9: Tracking efficiency for $e^+e^- \rightarrow t\bar{t}$ at $\sqrt{s} = 500 \text{ GeV}$ as a function of polar angle for (a) $0.5 \text{ GeV} < p_T < 2 \text{ GeV}$, (b) $2 \text{ GeV} < p_T < 30 \text{ GeV}$, and (c) $30 \text{ GeV} < p_T$ particles.

Similarly, when efficiency is plotted versus transverse momentum (figure 10), the modified detector exhibits greater efficiency for lower transverse momentum particles ($0.5 \text{ GeV} < p_T < 10 \text{ GeV}$) at low polar angle ($10^\circ < \theta$). This is evident in all three plots in figure 10 (figures 10a, 10b, 10c). However, as shown in figure 10c, for greater polar angles ($45^\circ < \theta$), once particles have transverse momentum $p_T > 20 \text{ GeV}$, Sidlo3 performs better, mirroring the performance as shown in figure 9c. For particles with $1 \text{ GeV} < p_T < 20 \text{ GeV}$, both detectors perform similarly well for polar angles ($\theta > 10^\circ$), evident in all three plots in figure 10.

Figure 11 illustrates the tracking efficiency for $e^+e^- \rightarrow t\bar{t}$ events as a function of the number hits generated by the Monte Carlo charged particle (figure 11a) and as a

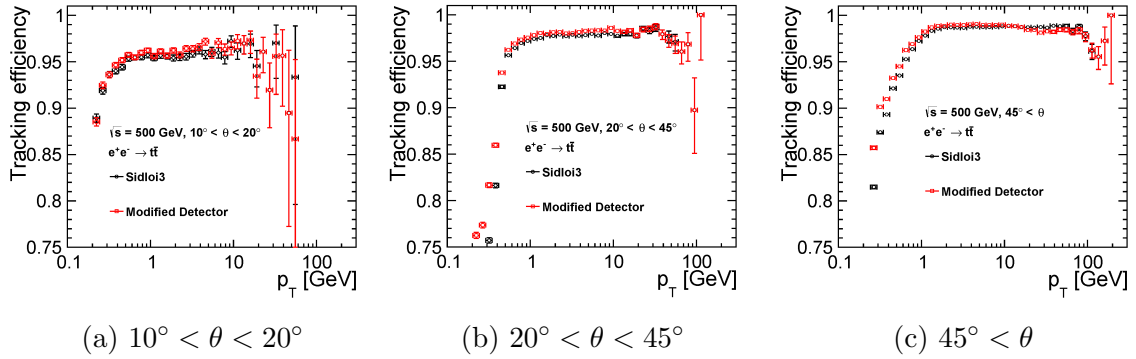


Figure 10: Tracking efficiency for $e^+e^- \rightarrow t\bar{t}$ at $\sqrt{s} = 500$ GeV as a function of transverse momentum for particles at (a) $10^\circ < \theta < 20^\circ$, (b) $20^\circ < \theta < 45^\circ$, and (c) $45^\circ < \theta$.

function of the distance to the closest hit of a different particle (figure 11b). Figure 11a illustrates that the modified detector has worse tracking efficiency for particles with < 12 hits. For particles with 12 hits, both detectors perform equally well, with efficiencies near 100%. The efficiency for both detectors drops for tracks with more than 12 hits, with the modified detector performing somewhat better for particles that produce 14 and 15 hits. The tracking efficiency with respect to the distance to the closest hit from another charged particle (figure 11b) is nearly equivalent for both detectors.

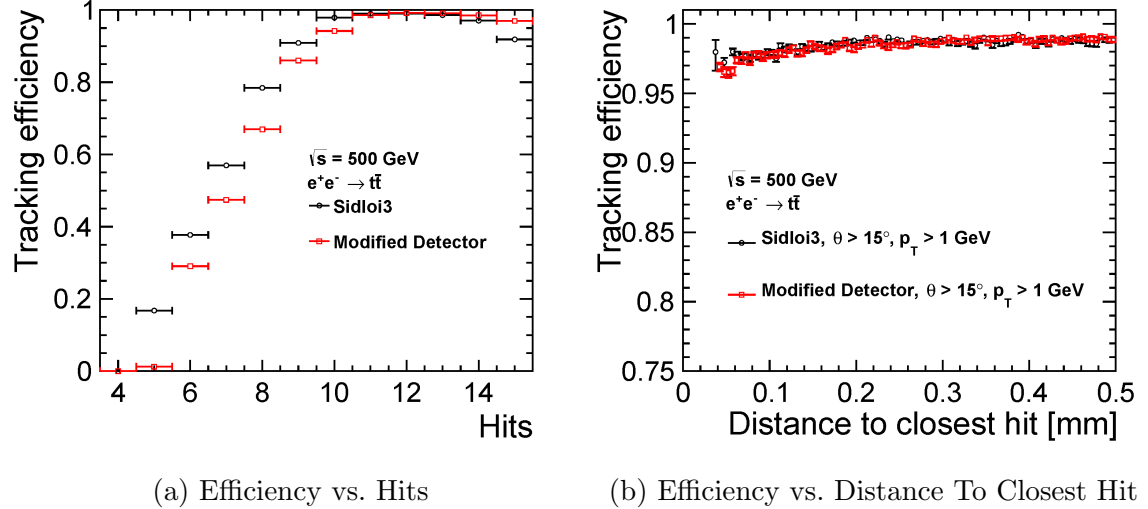


Figure 11: Tracking efficiency for $e^+e^- \rightarrow t\bar{t}$ at $\sqrt{s} = 500$ GeV as a function of (a) the total number hits generated by the Monte Carlo charged particle and (b) the distance to the closest hit generated by a different particle.

4.1.3 $e^+e^- \rightarrow t\bar{t}b\bar{b}$ (hadronic decays only), $\sqrt{s} = 1$ TeV

The tracking efficiencies for $e^+e^- \rightarrow t\bar{t}b\bar{b}$ events at $\sqrt{s} = 1$ TeV display most of the same trends as did the tracking efficiencies for the $\sqrt{s} = 500$ GeV $e^+e^- \rightarrow t\bar{t}$ events, albeit with some minor differences. To begin, the modified detector once again had greater efficiency for low transverse momentum particles ($0.5 \text{ GeV} < p_T < 2 \text{ GeV}$) for large polar angles ($\theta > 30^\circ$), as shown in figure 12a. In addition, the modified detector again had lower efficiency than SidloI3 for higher transverse momentum ($30 \text{ GeV} < p_T$) particles at $\theta > 60^\circ$ (figure 12c). Both results are similar to what is seen with the $e^+e^- \rightarrow t\bar{t}$ events in figure 9a and figure 9c, respectively. However, in the case of $e^+e^- \rightarrow t\bar{t}b\bar{b}$ events, both detectors had equal tracking efficiencies for particles with transverse momentum $2 \text{ GeV} < p_T < 30 \text{ GeV}$ (figure 12b) at polar angles $\theta > 45^\circ$. This is not the case for $e^+e^- \rightarrow t\bar{t}$ events (figure 9b), in which the modified detector has greater efficiency than SidloI3 for particles with transverse momentum $2 \text{ GeV} < p_T < 30 \text{ GeV}$ at polar angles $\theta > 45^\circ$. Still, note that there is a narrow polar angle region ($30^\circ < \theta < 45^\circ$) in figure 12b in which the modified detector did perform better than SidloI3, which agrees with the performance as shown for the $e^+e^- \rightarrow t\bar{t}$ events in figure 9b for that polar angle region.

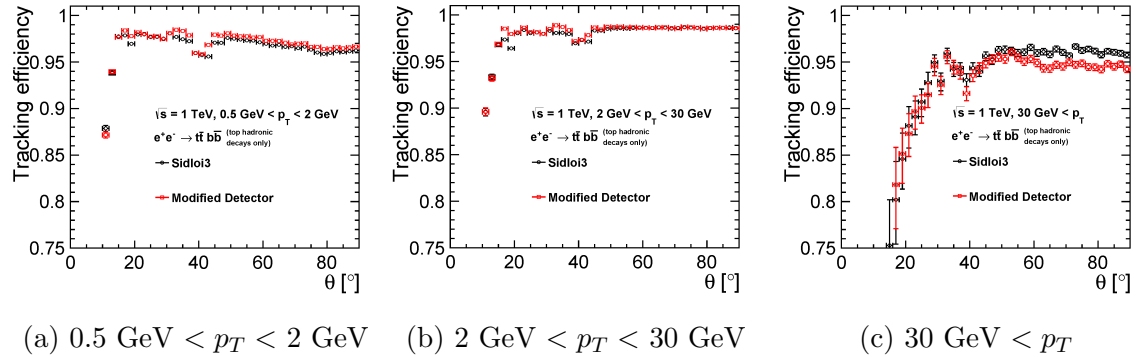


Figure 12: Tracking efficiency for $e^+e^- \rightarrow t\bar{t}b\bar{b}$ (hadronic decays only) at $\sqrt{s} = 1$ TeV as a function of polar angle for (a) $0.5 \text{ GeV} < p_T < 2 \text{ GeV}$, (b) $2 \text{ GeV} < p_T < 30 \text{ GeV}$, and (c) $30 \text{ GeV} < p_T$ particles.

Figure 13, in which efficiency is plotted versus transverse momentum for $e^+e^- \rightarrow t\bar{t}b\bar{b}$, supports the trends seen in figure 12. Figure 13c illustrates that the modified detector has worse efficiency for higher transverse momentum particles ($p_T > 20 \text{ GeV}$) at high polar angles ($\theta > 45^\circ$). Figure 13c and figure 13b also illustrate that the modified detector has better efficiency for lower transverse momentum ($0.2 \text{ GeV} < p_T < 1 \text{ GeV}$) particles at a wide polar angle ($\theta > 20^\circ$). In addition, the modified detector demonstrates slightly better efficiency for $1 \text{ GeV} < p_T < 10 \text{ GeV}$ particles

at $20^\circ < \theta < 45^\circ$, as shown in figure 13b. Unlike for the $e^+e^- \rightarrow t\bar{t}$ events as shown in figure 10a, the modified detector's improved efficiency for low transverse momentum ($0.2 \text{ GeV} < p_T < 2 \text{ GeV}$) particles does not extend to low polar angles ($10^\circ < \theta < 20^\circ$) for $e^+e^- \rightarrow t\bar{t}b\bar{b}$ events as is evident in figure 13a. Still, figure 13a indicates that the modified detector does have better efficiency for particles with slightly higher transverse momentum ($2 \text{ GeV} < p_T < 20 \text{ GeV}$) at low polar angles ($10^\circ < \theta < 20^\circ$), which agrees with figure 12.

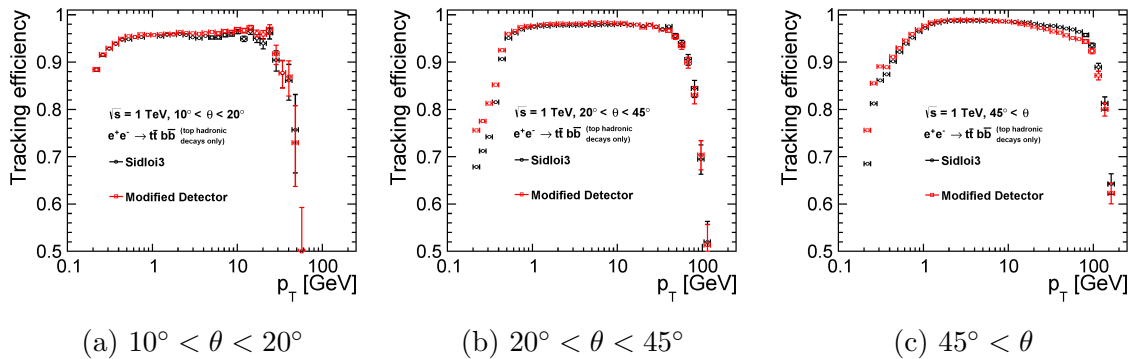


Figure 13: Tracking efficiency for $e^+e^- \rightarrow t\bar{t}b\bar{b}$ (hadronic decays only) at $\sqrt{s} = 1 \text{ TeV}$ as a function of transverse momentum for particles at (a) $10^\circ < \theta < 20^\circ$, (b) $20^\circ < \theta < 45^\circ$, and (c) $45^\circ < \theta$.

Efficiency versus total number of hits produced by the Monte Carlo charged particle is illustrated in figure 14a for $e^+e^- \rightarrow t\bar{t}b\bar{b}$ events. Again, the tracking efficiency for the modified detector is worse than that of SidloI3 for all particles which generated < 12 hits. Both detectors have nearly 100% tracking efficiency for particles generating 12 hits and slightly less efficiency for particles generating 13 or 14 hits, with the modified detector performing somewhat better for particles that produced 13 or 14 hits. This result is nearly identical to those in figure 11a for $e^+e^- \rightarrow t\bar{t}$ events. However, for efficiency versus the distance to the closest hit of a different particle (figure 14b), the modified detector clearly has worse tracking efficiency than SidloI3 from 0.02 mm to about 0.22 mm for $e^+e^- \rightarrow t\bar{t}b\bar{b}$ events. This stands in contrast to the results in figure 11b for the $e^+e^- \rightarrow t\bar{t}$ events, in which both detectors have comparably efficiency with respect to the distance to the closest hit from a different particle.

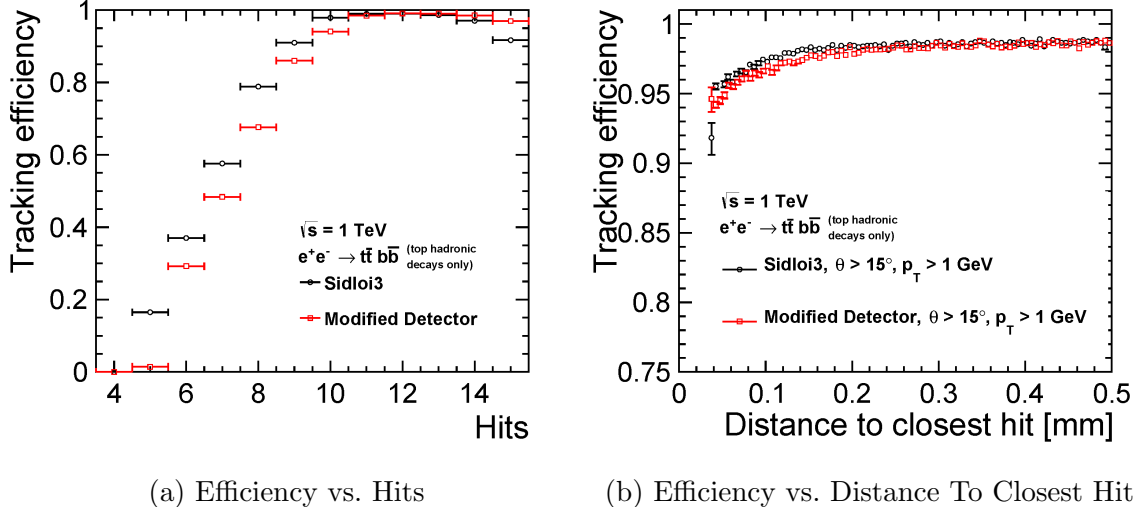


Figure 14: Tracking efficiency for $e^+e^- \rightarrow t\bar{t}b\bar{b}$ (hadronic decays only) at $\sqrt{s} = 1$ TeV as a function of (a) the number hits generated by the Monte Carlo particle associated with the track and (b) the distance from the track to the closest hit of another track.

4.2 Fake Rates

The fake rate is defined as the fraction of reconstructed tracks that have greater than one false hit:

$$\text{Fake Rate} = \frac{N_{\text{false hits} > 1}}{N_{\text{reconstructed}}}. \quad (2)$$

As figure 15 and figure 16 indicate, the modified detector demonstrates higher fake rates for both $e^+e^- \rightarrow t\bar{t}$ events at $\sqrt{s} = 500$ TeV and $e^+e^- \rightarrow t\bar{t}b\bar{b}$ events at $\sqrt{s} = 1$ TeV for polar angles $\theta > 25^\circ$ (figures 15a and 16a) and for transverse momentum $0.1 \text{ GeV} < p_T < 200 \text{ GeV}$ (figures 15b and 16b). At lower polar angles ($\theta < 25^\circ$), the distinction in performance between both detectors blurs for both types of physics events.

4.3 Impact Parameter Resolutions

4.3.1 Single Muons

For both detectors, the transverse impact parameter resolution improves as polar angle increases, and is better for higher momenta (figure 17a). In particular, for muons with $p \geq 10 \text{ GeV}$, transverse impact parameter resolution $\sigma(d_0)$ is better than $10 \mu m$ for polar angles $\theta > 20^\circ$ for both detectors. The transverse impact parameter

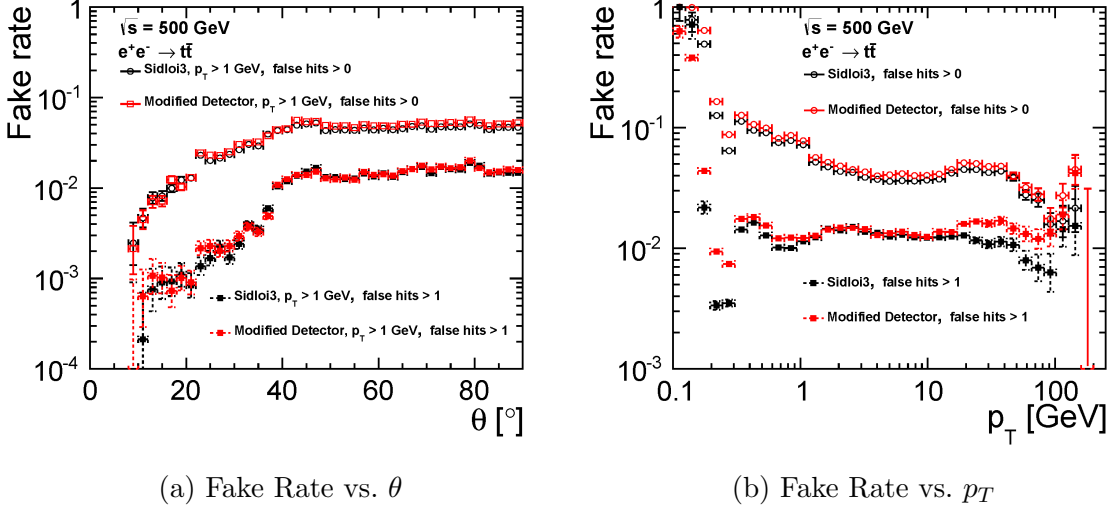


Figure 15: The fake rate of tracks for $e^+e^- \rightarrow t\bar{t}$ at $\sqrt{s} = 500$ GeV as a function of (a) polar angle and (b) transverse momentum.

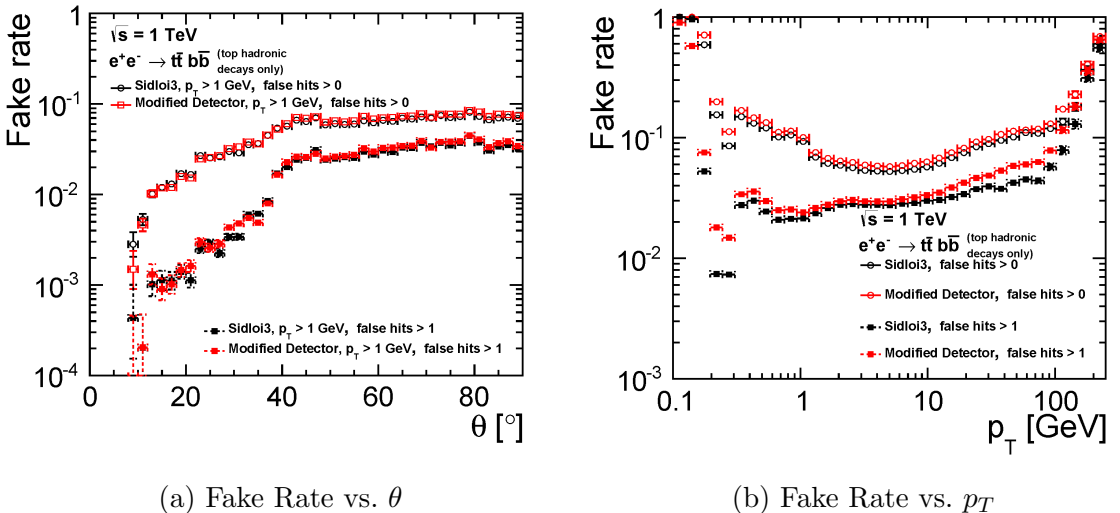


Figure 16: The fake rate on tracks for $e^+e^- \rightarrow t\bar{t}b\bar{b}$ (top hadronic decays only) at $\sqrt{s} = 1$ TeV as a function of (a) polar angle and (b) transverse momentum.

resolution improves to $4 \mu\text{m}$ for $p \geq 10 \text{ GeV}$ muons at polar angles $\theta > 50^\circ$ for both detectors. Muons with $p = 1 \text{ GeV}$ achieve transverse impact parameter resolution slightly greater than $10\mu\text{m}$ at $\theta = 90^\circ$. For lower polar angles ($\theta < 90^\circ$), the resolution worsens as with $p = 10 \text{ GeV}$ and 100 GeV muons.

Z -axis impact parameter resolution $\sigma(z_0)$ (figure 18a) also improves as polar angle increases and in general shows a greater dependence on polar angle, for both detectors. For low polar angles ($\theta \lesssim 35^\circ$), z -axis impact parameter resolution reaches values roughly an order of magnitude greater than transverse impact parameter resolution for $p = 1, 10$, and 100 GeV muons. However, as polar angle increases ($\theta > 40^\circ$), muons with $p = 1 \text{ GeV}$ demonstrate z -axis impact parameter resolution $\sigma(z_0)$ slightly greater than $10\mu\text{m}$, values nearly equal to the transverse impact parameter resolution for $p = 1 \text{ GeV}$ muons (figure 17a). As for $p = 10$ and 100 GeV muons, though z -axis impact parameter resolution does not quite reach as low as transverse impact parameter resolution for greater polar angles ($\theta > 40^\circ$), $\sigma(z_0)$ nevertheless reaches microns resolution for both detectors.

The ratio of the performance of the modified detector to the Sidlo3 benchmark,

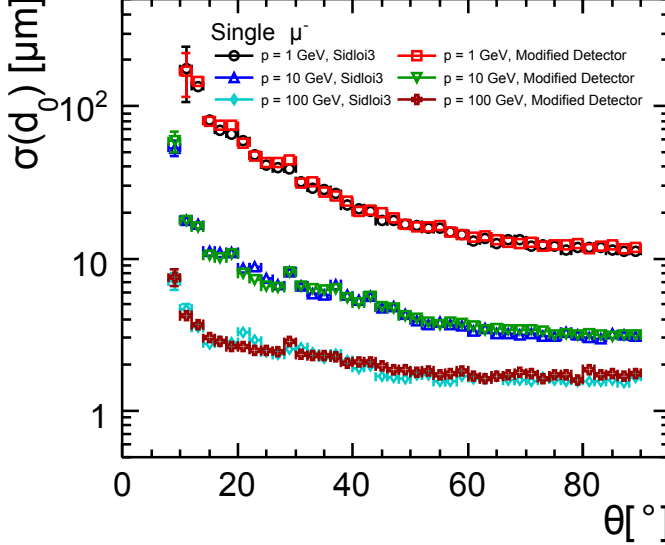
$$R = \frac{X_{\text{Modified Detector}}}{X_{\text{Sidlo3}}}, X = \sigma(d_0) \text{ or } \sigma(z_0), \quad (3)$$

is plotted in figure 17b for the transverse impact parameter resolution, $\sigma(d_0)$, and in figure 18b for the z -axis impact parameter resolution, $\sigma(z_0)$, for these momenta.

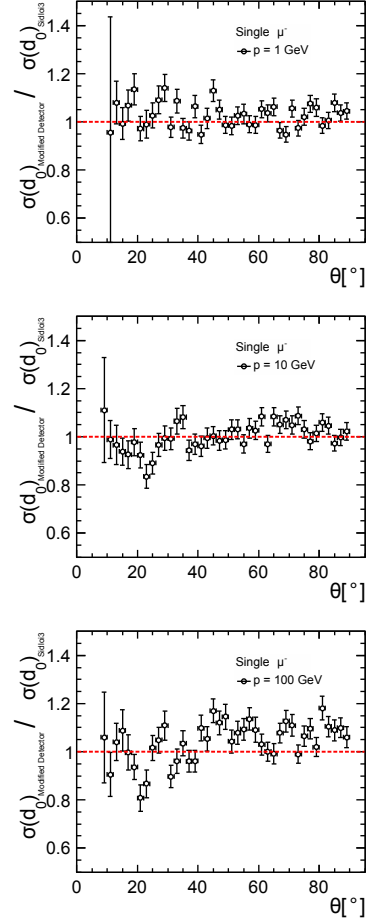
Figure 18a shows the z -impact parameter resolution for the two detector configurations. The unusual dip in z -impact parameter resolution at $\theta \approx 45^\circ$ for $p = 100 \text{ GeV}$ muons is due to the fact that the polar angle reconstruction does not use the outer tracker barrel hits, instead using only the vertex detector hits and the outer tracker disks. This results in a large increase in lever arm just before the barrel region ends (figure 4), which results in a rapid improvement of the z impact parameter resolution. As the lever arm continues to shorten as the polar angle increases ($\theta > 45^\circ$), the resolution starts worsening.

As figure 17b indicates, the transverse impact parameter resolution of the modified detector is usually worse for $p = 100 \text{ GeV}$ at $\theta > 45^\circ$ for muons with $p = 100 \text{ GeV}$. The modified detector performed better than Sidlo3 at $\theta > 20^\circ$. For muons with $p = 10 \text{ GeV}$, the modified detector performs better at lower polar angles ($\theta < 30^\circ$). At higher polar angles ($\theta > 30^\circ$), both detectors perform equally to within the error bars. Finally, for muons with $p = 1 \text{ GeV}$, both detectors performed equally to within error bars for a wide polar angle range ($10^\circ < \theta < 90^\circ$). In general, the modified detector tends to perform worse for higher polar angles and better for lower polar angles, also for high momenta.

Figure 18b shows the ratio of the z -impact parameter resolution for the two detec-



(a) $\sigma(d_0)$ vs. θ , both detectors



(b) $\sigma(d_0)$ ratio vs. θ

Figure 17: (a) Transverse impact parameter resolution as a function of polar angle for single muons of various energies for both detectors. (b) The ratio of the impact parameter resolutions as a function of polar angle.

tor configurations. In general, the modified detector demonstrates improved z -impact parameter resolution for large polar angles at high momenta. Specifically, for muons with $p = 100$ GeV, the modified detector has better $\sigma(z_0)$ for $\theta > 45^\circ$. For muons with $p = 10$ GeV, the polar angle range for improved z -axis parameter resolution falls to $\theta > 55^\circ$. On the other hand, for $p = 1$ GeV muons, the modified detector performs worse than SidloI3 for a wide polar angle ($25^\circ < \theta < 65^\circ$) and at no polar angle does performance dip in the modified detector's favor outside of the error bars, except slightly at $\theta \approx 25^\circ$.

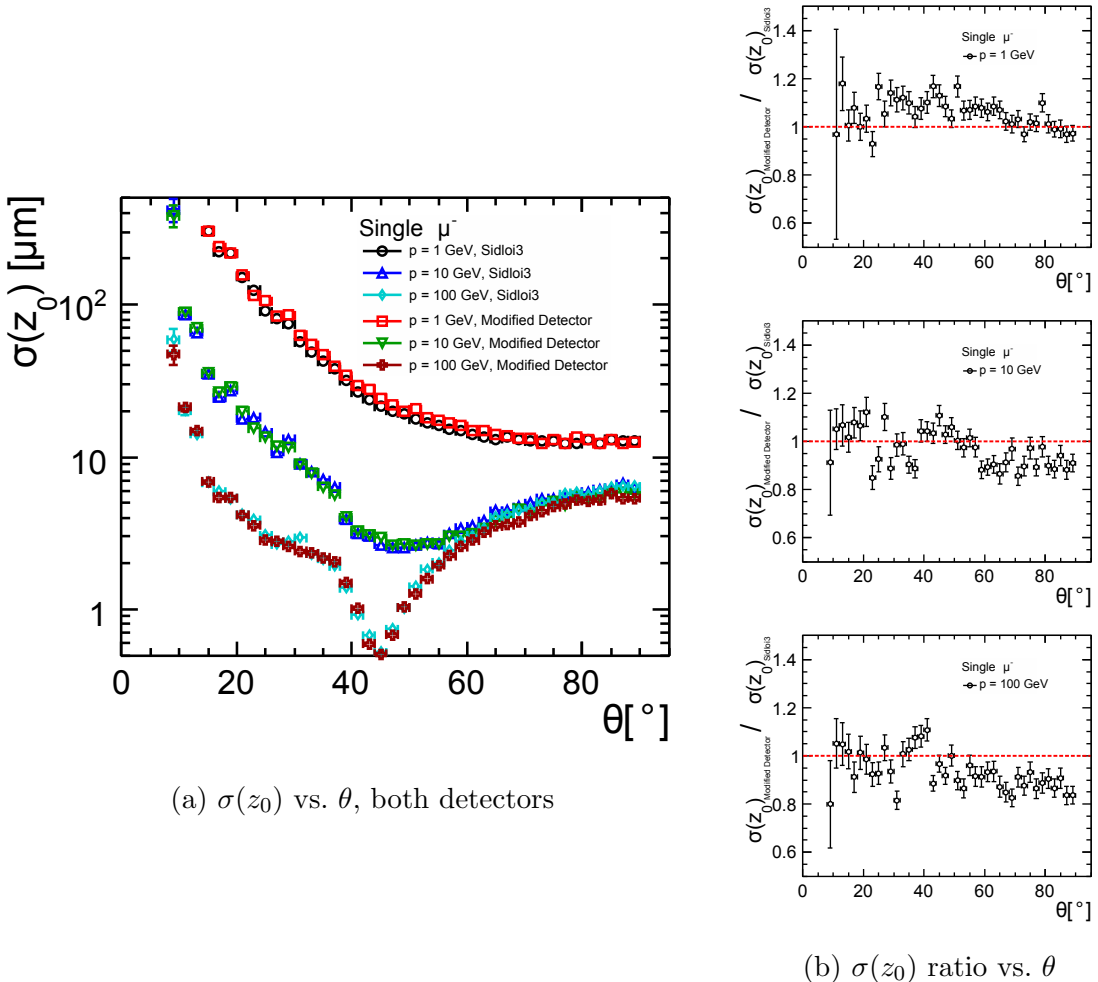


Figure 18: (a) Z -axis impact parameter resolution as a function of polar angle for single muons of various energies for both detectors. (b) The ratio of the impact parameter resolutions.

4.3.2 $e^+e^- \rightarrow t\bar{t}$, $\sqrt{s} = 500$ GeV

Figure 19 shows the transverse impact parameter resolution for both detectors with respect to polar angle for $e^+e^- \rightarrow t\bar{t}$ events. The trend is as seen for single muons (figure 17a). The resolution improves as polar angle increases, to $\sigma(d_0) \approx 10\mu m$. Furthermore, as figure 19b indicates, the performance of both detectors is nearly equal for a wide polar angle ($\theta > 35^\circ$). For $\theta < 35^\circ$, the modified detector performed slightly better than Sidlo3 for $20^\circ < \theta < 35^\circ$, and then Sidlo3 performed better for the relatively narrow polar angle $15^\circ < \theta < 20^\circ$.

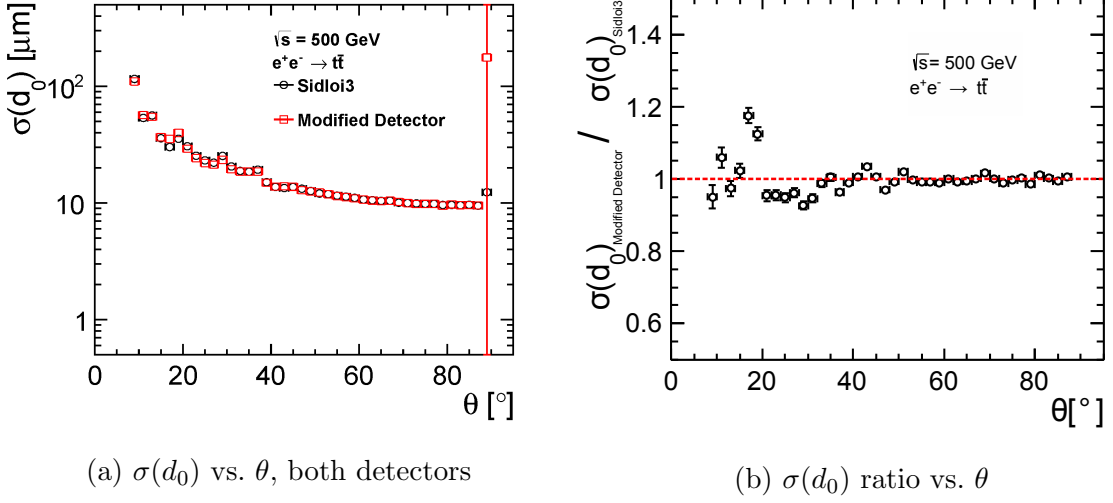


Figure 19: (a) Transverse impact parameter resolution as a function of polar angle for $e^+e^- \rightarrow t\bar{t}$ at $\sqrt{s} = 500$ GeV for both detector configurations. (b) The ratio of the impact parameter resolutions as a function of polar angle.

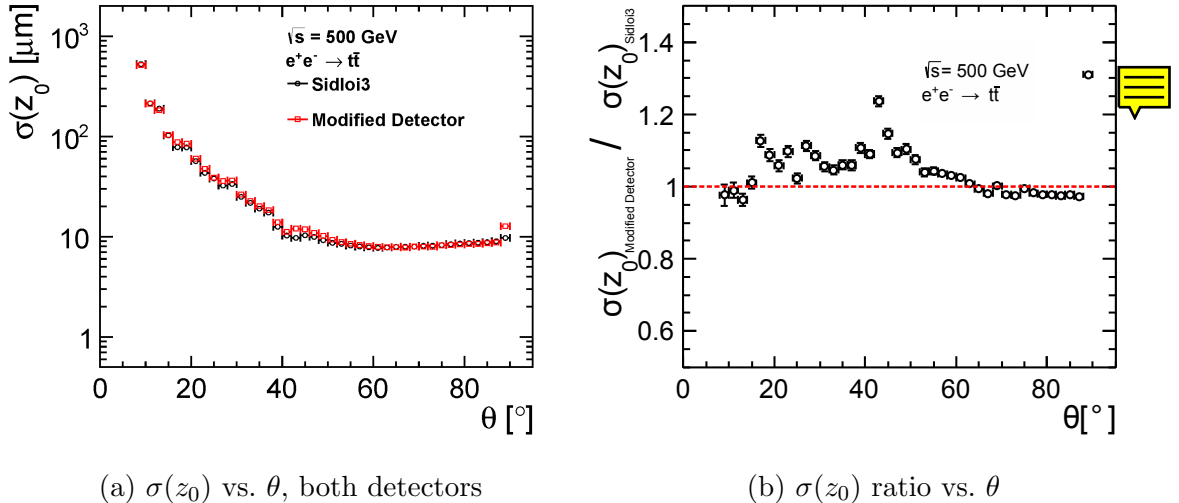


Figure 20: (a) Z -axis impact parameter resolution as a function of polar angle for $e^+e^- \rightarrow t\bar{t}$ at $\sqrt{s} = 500$ GeV for both detector configurations. (b) The ratio of the impact parameter resolutions as a function of polar angle.

The z -impact parameter resolution for $e^+e^- \rightarrow t\bar{t}$ events (figure 20a) also behaved as it did for single muons (figure 18a). The resolution reaches values $\approx 10\mu m$ as polar angle increases ($\theta > 40^\circ$) for both detectors. There is a decrease in z -axis impact parameter resolution right at $\theta = 90^\circ$ for both detectors, with the modified

detector demonstrating a greater increase. For lower polar angles ($\theta < 40^\circ$), $\sigma(z_0)$ decreases to values roughly an order of magnitude greater than transverse impact parameter resolution. However, the two detectors do not have equal performance with respect to z -impact parameter resolution, as figure 20b demonstrates. For a wide polar angle range ($20^\circ < \theta < 60^\circ$), the modified detector performs worse than SidloI3.

4.3.3 $e^+e^- \rightarrow t\bar{t}b\bar{b}$ (hadronic decays only), $\sqrt{s} = 1$ TeV

The $e^+e^- \rightarrow t\bar{t}b\bar{b}$ events displayed similar performance as the $e^+e^- \rightarrow t\bar{t}$ events with respect to both transverse impact parameter resolution (figure 21) and z -impact parameter resolution (figure 22) for both detectors. In particular, the transverse impact parameter resolution (figure 21) improved to $\sigma(d_0) \approx 10\mu m$ as the polar angle increased and also saw a decrease right at $\theta = 90^\circ$ that was worse for the modified detector than for SidloI3. Just as for the $e^+e^- \rightarrow t\bar{t}$ events, the two detectors performed equally well for $e^+e^- \rightarrow t\bar{t}b\bar{b}$ events with respect to $\sigma(d_0)$, albeit for a narrower polar angle range. In particular, their performances were equal for $30^\circ < \theta < 70^\circ$. For $\theta > 70^\circ$, the modified detector performed worse. For $20^\circ < \theta < 30^\circ$, the modified detector performed slightly better.

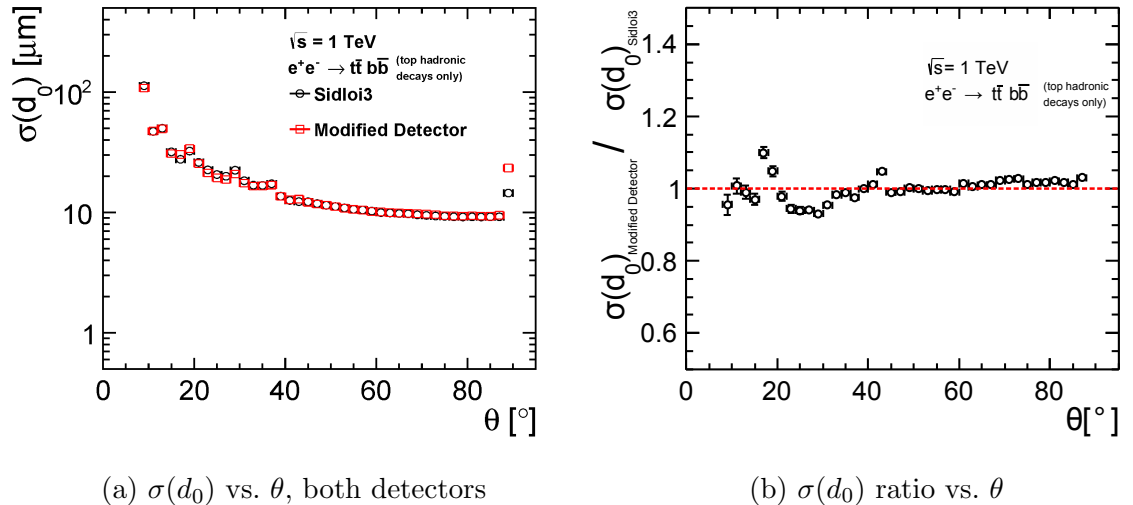


Figure 21: (a) Transverse impact parameter resolution as a function of polar angle for $e^+e^- \rightarrow t\bar{t}b\bar{b}$ at $\sqrt{s} = 1$ TeV for both detectors. (b) The ratio of the impact parameter resolutions as a function of polar angle.

The z -impact parameter resolution (figure 22), both detectors again reached $\approx 10\mu m$ for greater polar angles ($\theta > 40^\circ$) and were almost an order of magnitude worse

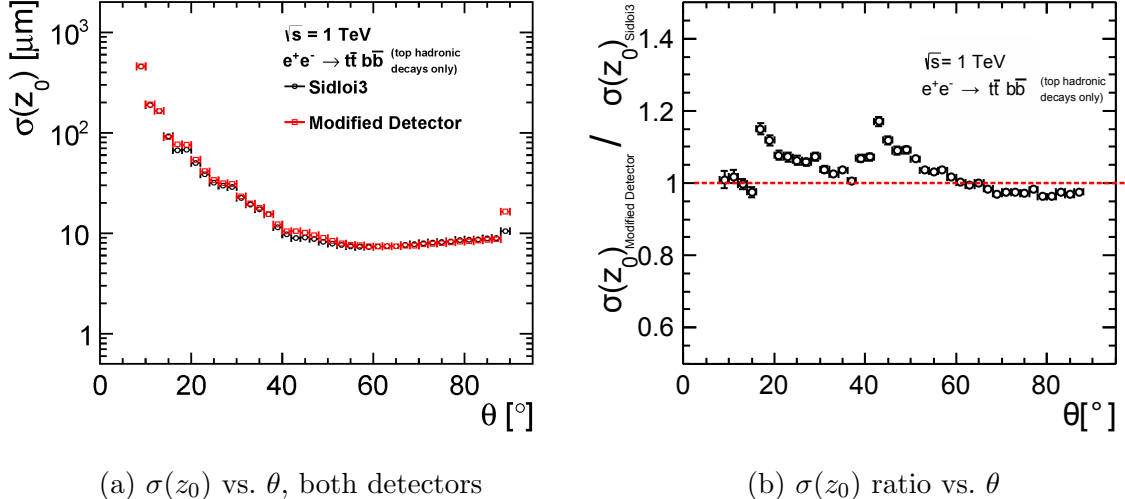


Figure 22: (a) Z -impact parameter resolution as a function of polar angle for $e^+e^- \rightarrow t\bar{t}bb$ at $\sqrt{s} = 1$ TeV for both detectors. (b) The ratio of the impact parameter resolutions as a function of polar angle.

than for $\sigma(d_0)$ at low polar angles ($\theta < 20^\circ$). Just as with the $e^+e^- \rightarrow t\bar{t}$ events, the ratio of the two detectors' z -axis impact parameter resolutions unequivocally shows regions in which one detector performs better than the other. As figure 22b shows, the modified detector had slightly better $\sigma(z_0)$ for $\theta > 65^\circ$. The modified detector had worse $\sigma(z_0)$ for $20^\circ < \theta < 65^\circ$.

4.4 Transverse Momentum Resolution

The transverse momentum resolution was fit according to the parameterization

$$\frac{\sigma(p_T)}{p_T^2} = a \oplus \frac{b}{p \sin \theta}, \quad (4)$$

where \oplus denotes addition in quadrature. As figure 23 illustrates, both detectors achieve a transverse momentum resolution $\sigma(p_T)/p_T^2 < 10^{-4}$ for $\theta > 30^\circ$ for high momentum ($p > 100$ GeV) tracks. For $\theta = 90^\circ$, both detectors achieve $\sigma(p_T)/p_T^2 < 10^{-5}$ for tracks with $p \gtrsim 200$ GeV. The transverse momentum resolution is comparable for both detectors.

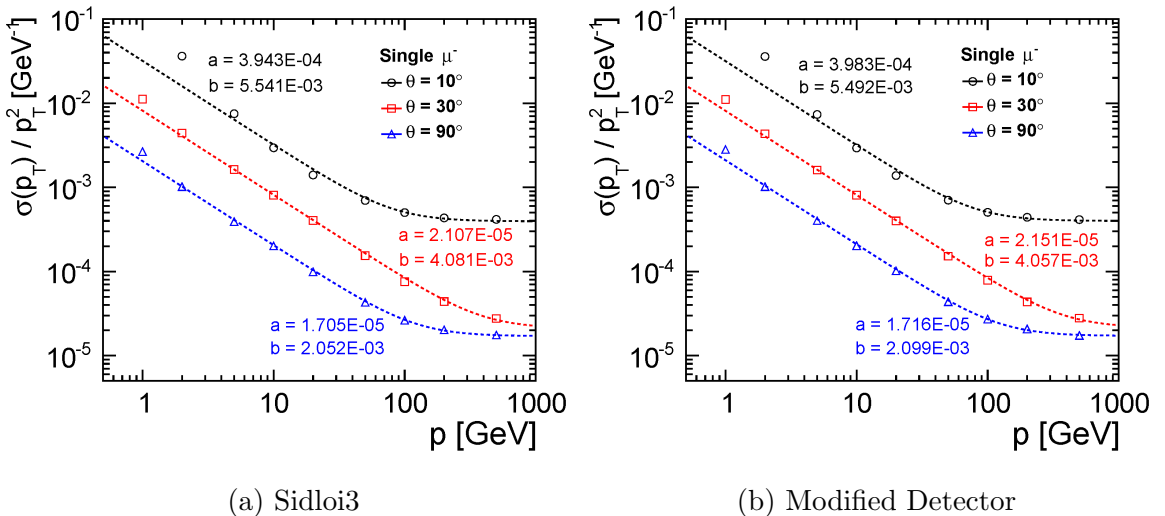


Figure 23: Transverse momentum resolution for single muons as a function of momentum for (a) SidloI3 and (b) the modified detector.

5 Discussion and Conclusion

The two vertex detector geometries show differences in tracking performance. However, the change in performance do not necessarily point to one geometry being an outright favorite over the other. In general, the tracking benefits achieved by the vertex barrel modification are outweighed by some other shortcoming.

For instance, though the modified detector had a higher tracking efficiency for low momentum particles in both physics processes ($e^+e^- \rightarrow t\bar{t}$ at $\sqrt{s} = 500$ GeV, figure 9a; $e^+e^- \rightarrow t\bar{t}bb$ (hadronic decays only) at $\sqrt{s} = 1$ TeV, figure 12a), the modified detector had a higher fake rate for reconstructed tracks (figure 15, figure 16). Therefore, even though the modified detector will reconstruct a greater number of tracks, those additional tracks will more often contain mismatched hits from other Monte Carlo particles than they would have had Sidlo3 reconstructed them because Sidlo3 has a lower fake rate. Furthermore, the modified detector's higher efficiency for lower momentum particles is again outweighed by the modified detector's lower efficiency for high momentum particles (figure 9c, figure 12c) and lower efficiency with respect to the number of hits produced the Monte Carlo charged particle (figure 11a, figure 14a).

In addition, though modified detector exhibited better z -axis impact parameter resolution $\sigma(z_0)$ for 10 and 100 GeV muons at high polar angles (figure 18b), it also demonstrated worse z -axis impact parameter resolution for 1 GeV muons at lower polar angles (figure 18b) and worse transverse impact parameter resolution $\sigma(d_0)$ for

10 and 100 GeV muons at high polar angles (figure 17b). For the physics processes, though both detectors had equal transverse impact parameter resolution for a wide polar angle (figure 19b, figure 21b), the modified detector had worse z -axis impact parameter resolution for a wide range of polar angles (figure 20b, figure 22b). The modified detector’s increased z -axis impact parameter resolution for high energy single muons (figure 18b) was present for the two physics processes (figure 20b, figure 22b) but to a lesser extent.

The difference in tracking performance between the two vertex detector layouts indicates that the modified vertex barrel geometry is not optimal. However, it also suggests that the baseline SidloI3 vertex geometry might not be optimal, since by some measures the modified detector performed better. Further studies, with for instance hybrid vertex barrel geometries that mix doublet tracking and single tracking layers or that have reduced material budgets, should be conducted to see if it is possible to achieve the improvements demonstrated by the modified detector without compromising the strong performance of the baseline vertex detector. Moreover, studies with a different geometry of the outer tracker should also be conducted, so as to pave the road for optimizing the entire tracking system for SiD.

References

- [1] T. Behnke, J. E. Brau, P. N. Burrows, J. Fuster, M. Peskin, *et al.*, “The International Linear Collider Technical Design Report - Volume 4: Detectors” [arXiv:1306.6329 \[physics.ins-det\]](https://arxiv.org/abs/1306.6329).
- [2] H. Baer, T. Barklow, K. Fujii, Y. Gao, A. Hoang, *et al.*, “The International Linear Collider Technical Design Report - Volume 2: Physics” [arXiv:1306.6352 \[hep-ph\]](https://arxiv.org/abs/1306.6352).
- [3] T. G. White, “Performance studies of a pixel tracker in the Silicon Detector (SiD) concept for a future linear collider” *ArXiv e-prints* (Apr., 2011) , [arXiv:1104.4547 \[physics.ins-det\]](https://arxiv.org/abs/1104.4547).
- [4] N. Graf and J. McCormick, “Simulator for the linear collider (slic): a tool for ilc detector simulations” in *AIP Conf. Proc. 867: 503-512, 2006*, no. SLAC-PUB-12350, Stanford Linear Accelerator Center (SLAC). 2007.
- [5] S. Agostinelli, J. Allison, K. E. Amako, J. Apostolakis, H. Araujo, P. Arce, M. Asai, D. Axen, S. Banerjee, G. Barrand, *et al.*, “Geant4a simulation toolkit” *Nuclear instruments and methods in physics research section A: Accelerators, Spectrometers, Detectors and Associated Equipment* **506** (2003) no. 3, 250–303.
- [6] J. Allison, K. Amako, J. Apostolakis, H. Araujo, P. A. Dubois, M. Asai, G. Barrand, R. Capra, S. Chauvie, R. Chytracek, *et al.*, “Geant4 developments and applications” *Nuclear Science, IEEE Transactions on* **53** (2006) no. 1, 270–278.
- [7] “Linear collider simulation” 2014. <http://www.lcsim.org/sites/lcsim/index.html>.
- [8] N. A. Graf, “org.lcsim: Event reconstruction in java” in *Journal of Physics: Conference Series*, vol. 331, p. 032012, IOP Publishing. 2011.

- [9] C. Grefe, S. Poss, A. Sailer, A. Tsaregorodtsev, the Clic detector, and physics study, “Ilcdirac, a dirac extension for the linear collider community” *Journal of Physics: Conference Series* **513** (2014) no. 3, 032077. <http://stacks.iop.org/1742-6596/513/i=3/a=032077>.
- [10] A. Tsaregorodtsev, M. Bargiotti, N. Brook, A. C. Ramo, G. Castellani, P. Charpentier, C. Cioffi, J. Closier, R. G. Diaz, G. Kuznetsov, *et al.*, “Dirac: a community grid solution” in *Journal of Physics: Conference Series*, vol. 119, p. 062048, IOP Publishing. 2008.
- [11] F. Gaede, T. Behnke, N. Graf, and T. Johnson, “LCIO: A persistency framework for linear collider simulation studies” *ArXiv Physics e-prints* (June, 2003) , [physics/0306114](https://arxiv.org/abs/physics/0306114).
- [12] “Stdhep” 2013. <http://cepa.fnal.gov/psm/stdhep/>.
- [13] W. Kilian, T. Ohl, and J. Reuter, “Whizard: simulating multi-particle processes at lhc and ilc” *The European Physical Journal C* **71** (2011) no. 9, 1–29.
- [14] T. Sjöstrand, S. Mrenna, and P. Skands, “Pythia 6.4 physics and manual” *Journal of High Energy Physics* **2006** (2006) no. 05, 026.
- [15] C. Grefe, “Detector Optimization Studies and Light Higgs Decay into Muons at CLIC” [arXiv:1402.2780 \[physics.ins-det\]](https://arxiv.org/abs/1402.2780).
- [16] “Geant4 physics reference manual” 2011. <http://cepa.fnal.gov/psm/stdhep/>.
- [17] S. Piparov, “Geant4 validation with CMS calorimeters test-beam data” *ArXiv e-prints* (Aug., 2008) , [arXiv:0808.0130 \[physics.ins-det\]](https://arxiv.org/abs/0808.0130).
- [18] M. Krammer and H. Pernegger, “Signal collection and position reconstruction of silicon strip detectors with 200 μm readout pitch” *Nuclear Instruments and Methods in Physics Research Section A: Accelerators, Spectrometers, Detectors and Associated Equipment* **397** (1997) no. 2, 232–242.
- [19] T. Krämer, “Track parameters in lcio” tech. rep., LC-DET-2006-004, 2006.
- [20] J. Alcaraz, “Helicoidal tracks” tech. rep., L3 Note 1666, February 1995, 1995.